frontiers | Frontiers in Chemical Engineering

TYPE Original Research
PUBLISHED 22 February 2024
DOI 10.3389/fceng.2024.1334355

OPEN ACCESS

EDITED BY
Jose Escobar,
Mexican Institute of Petroleum, Mexico

REVIEWED BY
María Barrera,
Universidad Veracruzana, Mexico
Luděk Kaluža,
Institute of Chemical Process Fundamentals (ASCR), Czechia

*CORRESPONDENCE
J. A. Melo-Banda,
aaron.mb@cdmadero.tecnm.mx

RECEIVED 07 November 2023
ACCEPTED 15 January 2024
PUBLISHED 22 February 2024

CITATION
Guerrero-Corona CE, Melo-Banda JA, Lam-Maldonado M, Vega-Ibarra LA, Diaz-Zavala NP and Meraz-Melo MA (2024), Transition metal oxide nanocatalysts for the deoxygenation of palm oil to green diesel. *Front. Chem. Eng.* 6:1334355. doi: 10.3389/fceng.2024.1334355

Transition metal oxide nanocatalysts for the deoxygenation of palm oil to green diesel

C. E. Guerrero-Corona[1], J. A. Melo-Banda[1]*, M. Lam-Maldonado[1], L. A. Vega-Ibarra[1], N. P. Diaz-Zavala[1] and M. A. Meraz-Melo[2]

[1]Tecnológico Nacional de México/Campus Cd. Madero, Centro de Investigación en Petroquímica, Prolongación Bahía Aldair, Blvd. De las Bahias, Parque Industrial Tecnía, Altamira, México, [2]Tecnológico Nacional de México/Campus Puebla, División de Estudios de Posgrado e Investigación, Puebla, México

This study investigated the hydrodeoxygenation of palm oil by different oxide nanocatalysts of transition metals α -Fe_2O_3, NiO, and $NiFe_2O_4$, which were synthesized by hot injection. All nanomaterials were characterized by X-ray diffraction, Fourier transform infrared spectroscopy, and dynamic light dispersion. The catalytic evaluation was performed in a Parr-type reactor at 350°C, 3.5 MPa of H_2 pressure, and 3 h of reaction. The liquid product obtained was analyzed by ultraviolet-visible light spectroscopy to identify the n-C_{16} generated during the reaction. The activity in the deoxygenation of fatty acids to produce n-C_{16} hydrocarbons has the following order: α-Fe_2O_3 < $NiFe_2O_4$ < NiO.

KEYWORDS

nanocatalysts, transition metal oxide, palm oil, deoxygenation, green diesel

1 Introduction

Deriving green diesel from the deoxygenation of vegetable oils has attracted attention due to the high increment of sulfur, nitrogen, oxygen, and metal heterocompounds in oil reserves, the high demand for fossil fuels, and the environmental problems they generate (Demirbas, 2004; Demirbas and Dincer, 2008). Therefore, it has become necessary to develop a green and renewable alternative that can be a substitute for petroleum-derived fuels. A wide variety of vegetable oils, such as soja, sunflower, jatropha, and palm (Guzman et al., 2010; Gong et al., 2012; Kim et al., 2013), have been used as feedstock for the production of this green diesel (Guzman et al., 2010; Gong et al., 2012; Kim et al., 2013). In particular, the molecular composition of palm oil contains mostly fatty acids such as C_{16} and C_{18}, making it a promising feedstock (Srifa et al., 2014) because it contains relatively low concentrations of oxygen, which makes it very desirable for the production of hydrocarbons in the conventional diesel range. In addition, the fatty acid or triglyceride contents in certain oils (not edible) could be an alternative for producing clean n-C_{16}. Green diesel has gained increased interest due to it being considered superior to fossil diesel and biodiesel. One of its most important attributes is a higher cetane index (ignition capacity in a certain period of time) because it does not contain oxygen in its molecules and has a high calorific value (Vonortas and Papayannakos, 2014). It is obtained by deoxygenation, hydrodeoxygenation (HDO), decarbonylation (DCO), and the decarboxylation (DCO_2) of oil in the presence of hydrogen, high temperature (300°C–360 °C), H_2 pressure (>3 MPa), and catalysts, which

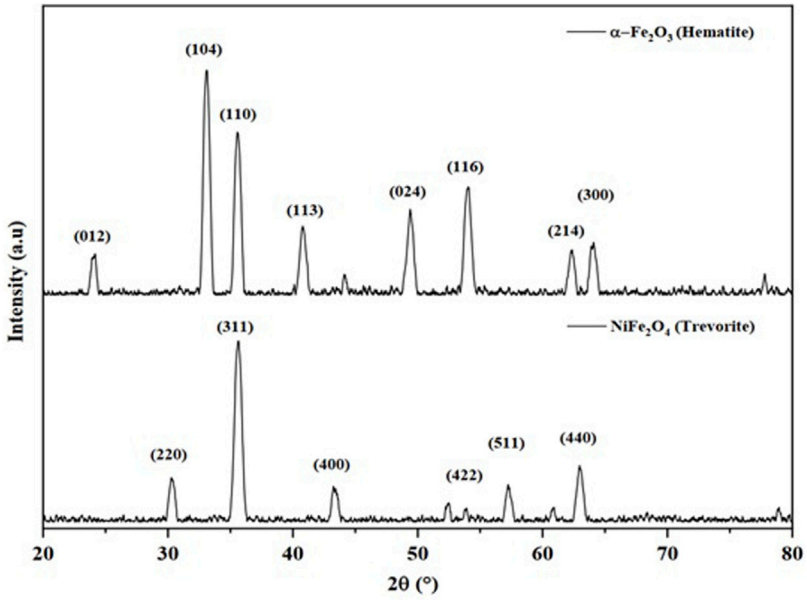

FIGURE 1
X-ray-diffractogram pattern of α-Fe_2O_3 and $NiFe_2O_4$ nanocatalysts.

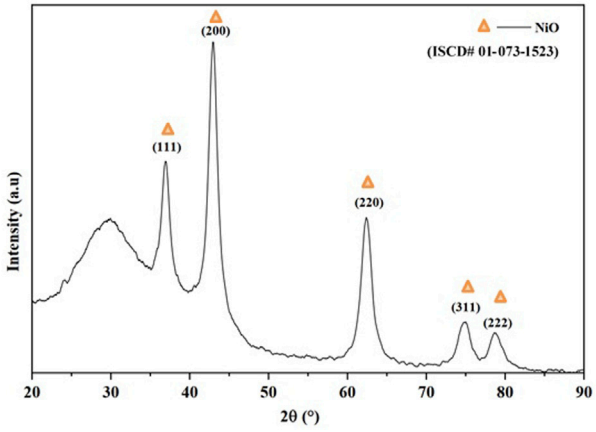

FIGURE 2
X-ray-diffractogram pattern of the NiO nanocatalyst.

TABLE 1 Crystalline phases from X-ray diffraction of the synthesized nanocatalysts.

Parameter	α-Fe_2O_3	NiO	$NiFe_2O_4$
Crystalline phase	Rhombohedral	Cubic	Cubic
Crystallite size	15.98 nm	5.5 nm	13.93 nm

efficiently promote such reactions (Kovács et al., 2011; Morgan et al., 2012; Kubička et al., 2014; Srifa et al., 2015a; Srifa et al., 2015b). Therefore, the main objective of this research was to synthesize α-Fe_2O_3, $NiFe_2O_4$, and NiO nanocatalysts using the hot injection process, with only oleylamine as a surfactant, solvent, and reducing agent, as well as the catalytic evaluation of the deoxygenation of palm oil for the production of molecules in the diesel range.

2 Materials and methods

2.1 Materials

Iron acetylacetonate (III) ($Fe(C_5H_7O_2)_3$, 97%), nickel acetylacetonate (II) ($Ni(C_5H_7O_2)_2$, 95%), oleylamine ($C_{18}H_{37}N$, technical grade, 70%) as reductor agent during the synthesis, ethanol (C_2H_6O, 99.9%) acquired in Sigma-Aldrich as the chemical solvent to remove organic residues from synthesis, heptane (n-C_7, 99%) (Sigma-Aldrich), and toluene ($C_6H_5CH_3$, 99.5%) acquired in Fermont were used as solvents in catalytic tests. Hexadecane (n-C_{16}, 99%) (Sigma-Aldrich) was used as standard performance calibration for product analysis.

2.2 Methods

2.2.1 Preparation of catalysts

The nanomaterials were synthesized using hot injection. This method consisted of preheating the solvent oleylamine below its boiling point with a heating ramp of 20 °C/min and then adding the organometallic precursors. In general, for α -Fe_2O_3 catalysts, 2 mmol of the precursor $Fe(acac)_3$ was added to the previously heated solvent, and the solution was kept under continuous agitation for 2 h. Next, for the NiO particles, 2 mmol of the precursor $Ni(acac)_2$ was used in oleylamine with a reaction time of 2 h.

Finally, to synthesize the $NiFe_2O_4$ nanocatalysts, the same method was used slightly differently. The precursors were added in a 2:1 M ratio of $Fe(acac)_3$ and $Ni(acac)_2$ to the solvent to form a mixture and were kept under agitation for 3 h. The resulting solution from each reaction was

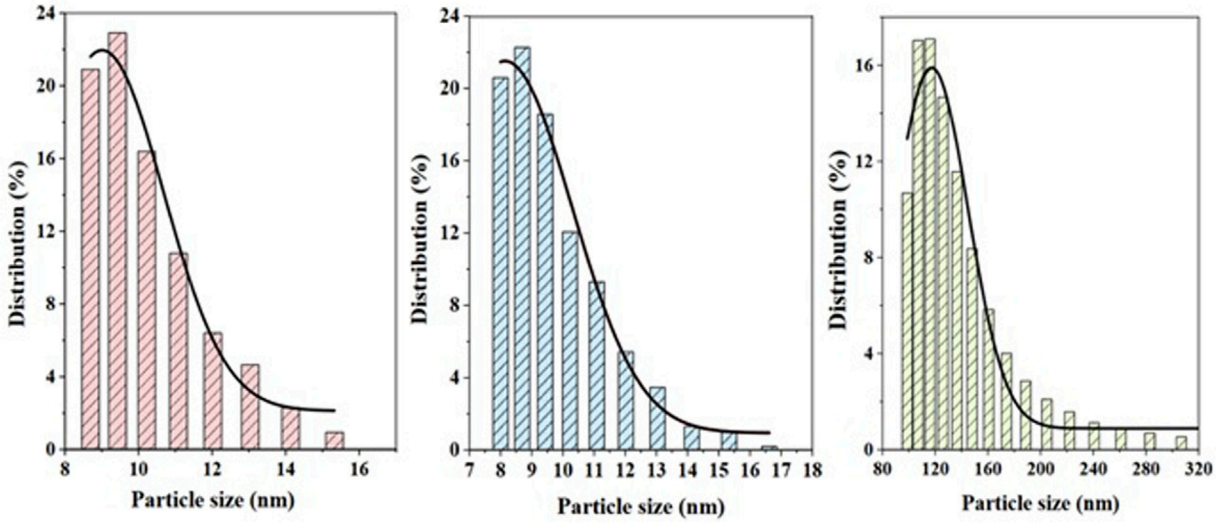

FIGURE 3
Particle size distribution for **(A)** α-Fe_2O_3, **(B)** $NiFe_2O_4$, and **(C)** NiO nanomaterials.

removed from the heat source and allowed to cool to room temperature before any additional steps. Finally, the product was divided into three equal parts and deposited in 50-mL centrifuge tubes. Ethanol was added to each sample and centrifuged at 6,000 rpm for 25 min. At the end of centrifugation, the precipitate was collected and repeatedly washed with solvent to remove the residues from the reaction. Final samples were calcinated from room temperature to 673 K at 20 K/min over 2 h.

2.2.2 Characterization methods

The crystal structure of the synthesized materials was obtained by X-ray diffraction (XRD) with a Bruker D8 Advance diffractometer under the following experimental conditions: CuKα radiation, 40 kV, and 30 mA, in a range of 2θ between 10° and 70°. The identification of the phase and crystal structure of each sample was determined using X'Highscore Plus software, version 3.0.5. Using the Debye–Scherrer equation, the crystal size for all synthesized samples was determined. Information was obtained on the functional groups present and the interactions between the bonds of the stabilizing molecules and the nanoparticles by FTIR spectroscopy in a Perkin Elmer spectrophotometer, Spectrum 100 model. The analyses were carried out in the mid-infrared region (4,000–500 cm^{-1}). In addition, the distribution of the average size of the suspended particles was determined using the dynamic light dispersion technique with Anton Paar Litesizer 500 equipment and software. For this technique, the samples were prepared at a concentration of 0.1 mg/mL. JEOL, STEM J-7600 equipment was used to analyze the morphologic and particle size in the samples.

2.2.3 Catalytic deoxygenation tests

Catalytic deoxygenation tests were conducted in a batch reactor type Parr model 4,577. Each experiment was carried out with 26 mL of palm oil, 80 mL of n-heptane, and 1,000 ppm of the three different catalysts. The reactor was purged for 10 min with nitrogen to remove the air and then pressurized with hydrogen. The reaction conditions were 350 °C for 3 h and 3.5 MPa of H_2 pressure. The agitation remained constant at 250 rpm to ensure the total dispersion of the nanocatalysts in the oil. A calibration curve was used to identify the n-C_{16} hydrocarbon generated during the reaction. A 1,000 mg·L^{-1} quantity of n-C_{16} stock solution had been previously prepared in toluene and dissolved in different concentrations. Changes in concentration were determined with the UV-vis spectrophotometer, Model Agilent Technologies-Carry-60. The initial concentrations for the calibration curve were solutions from 10 mg·L^{-1} to 60 mg·L^{-1}. In brief, 1 μL of the sample was diluted in 100 mL of toluene, and the measurements were conducted to determine the n-alkane (n-C_{16}) generated during the reaction.

3 Results and discussions

3.1 X-ray diffraction

The diffractogram of the materials synthesized from $Fe(acac)_3$ is shown in Figure 1. The diffraction pattern indicates a rhombohedral structure (space group R-3, number 148). The peaks in 2θ = 24.125°, 33.115°, 35.612°, 40.836°, 49.417°, 54.005°, 62.385°, and 63.966° assigned to the planes (012), (104), (110), (113), (024), (116), (214), and (300) are characteristic of hematite phase α-Fe_2O_3 (PDF# 00-024-0072). By mixing the previous precursors of $Fe(acac)_3$ and $Ni(acac)_2$ in a 2:1 ratio, a cubic structure belonging to the space group Fd3m, number 227, was obtained. According to the diffraction peaks located in the plane, 2θ = 30.29°, 35.68°, 43.36°, 53.81°, 57.37°, and 63°, corresponding to the planes (220), (311), (400), (422), (511), and (440), are characteristic of the $NiFe_2O_4$ trevorite phase [PDF# 00-04, ISCD# 01-073-1523]. In both cases, the results were consistent with previous investigations (Belaïd et al., 2013; Kurtan et al., 2016; Babu and Reddy, 2020; Dippong et al., 2021). Figure 2 shows the diffractogram of the nanocatalysts synthesized from the organometallic precursor $Ni(acac)_2$. The diffraction pattern indicates a cube structure centered on the faces (fcc) (space group Fm-3m, number 225). The peaks in 2θ = 37.22°, 43.25°, 62.83°, 75.35°, and 79.34° assigned to the planes (111), (200), (220), (311), and (222) correspond to NiO (ISCD# 01-073-1523). The same structure was reported in Gutierrez et al. (2013).

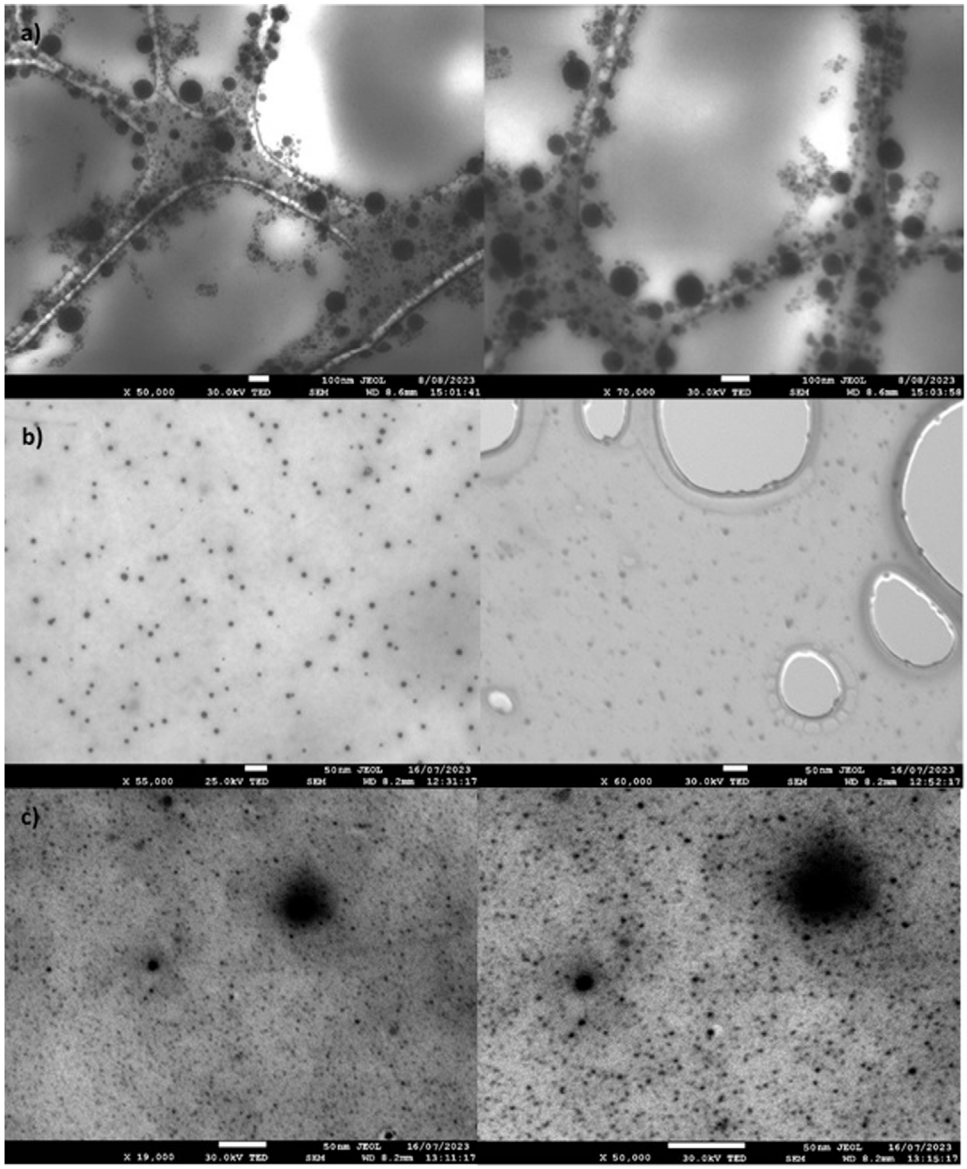

FIGURE 4
TEM micrographs of **(A)** NiO, **(B)** α-Fe_2O_3, and **(C)** $NiFe_2O_4$ nanomaterials.

Using the Debye–Scherrer equation, the size of the crystal was determined for all the synthesized samples (Cullity and Stock, 2013). It was obtained from the maximum half-height width (FWHM) of the plane (104) α-Fe_2O_3, (200) NiO, and (311) $NiFe_2O_4$. For hematite and trevorite samples, the crystal size is equivalent to the particle size, suggesting a minimal form as a monocrystalline material. NiO catalysts are composed of 5.5 nm nanocrystals and have an average particle size of 146 nm, so it can be determined that it is a polycrystalline material. The summary of the DRX results is shown in Table 1.

3.2 Dynamic light dispersion

The particle size distribution of the α-Fe_2O_3, NiO, and $NiFe_2O_4$ catalysts obtained by dynamic light dispersion is shown in Figure 3. The pink histogram shows particle sizes for hematite between 8 and 15 nm, with an average size of 11.74 nm. Trevorite catalysts have similar particle sizes of 8–17 nm and an average size of 12.28 nm, as can be seen on the blue histogram. NiO catalysts, unlike the previous two materials, have sizes between 100 and 280 nm caused by their possible agglomeration. This behavior was reported previously by Lam et al. (2020).

3.3 Transmission electronic microscopy

Figure 4 shows the micrographs of NiO, Fe_2O_3, and $NiFe_2O_4$ nanocatalysts. In general, the three micrographed materials exhibit particle sizes less than 50 nm; however, in two materials containing nickel, the presence of particles larger than 70–80 nm can be observed, attributed to agglomerations of smaller particles (Maity et al., 2009; Pan et al., 2014; Lam et al., 2020). Similar results were reported in DLS analyses, with smaller sizes and large

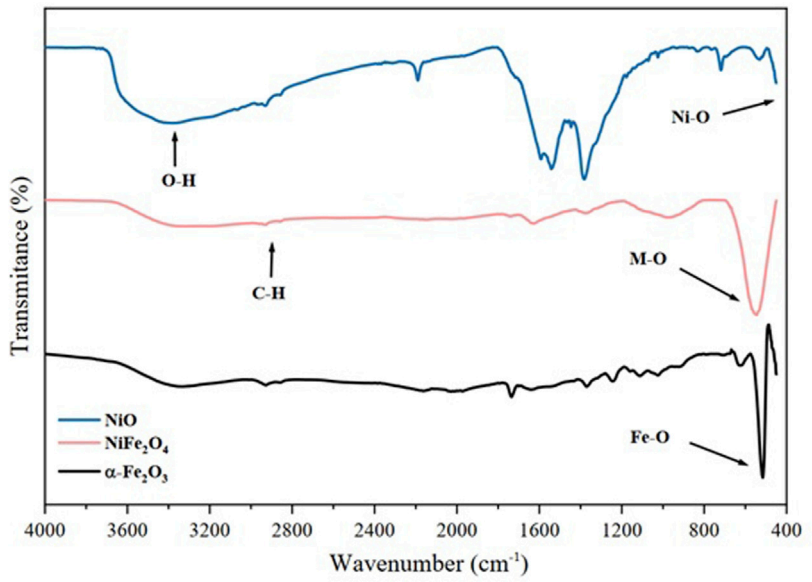

FIGURE 5
FTIR spectra of α-Fe_2O_3, $NiFe_2O_4$, and NiO nanocatalysts.

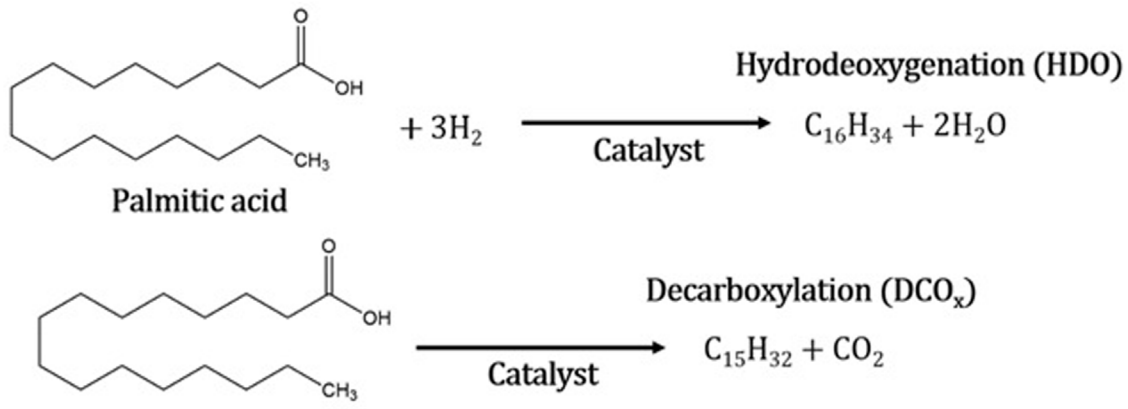

FIGURE 6
Possible reaction pathways for green diesel production.

particle size (>100 nm) attributable to the agglomeration of small particles. These differences were attributed to the precursors and reagents used in the synthesis. Furthermore, the micrographs for Fe_2O_3 and $NiFe_2O_4$ show the presence of nanoparticles less than 20 nm.

3.4 IR spectroscopy

The nanomaterials were analyzed by IR spectroscopy to determine the functional groups present on the surface. Figure 5 shows the spectra of the nanocatalysts of α-Fe_2O_3, NiO, and $NiFe_2O_4$ in the range of 4,000 to 400 cm^{-1}. All the samples analyzed exhibit bands between 2,922 cm^{-1} and 2,854 cm^{-1} that correspond to the symmetrical (vs.) and asymmetric (ν_{as}) stretching vibrations of the groups (C–H) (Mourdikoudis and Liz-Marzán, 2013). These assignments are attributed to the oleylamine used in the synthesis of the material, indicating the presence of amino groups on the surface of the catalysts, which provide stability and prevent them from agglomerating (Zhai et al., 2012). The bands between 500 and 400 cm^{-1} correspond to the strong vibrations of the metal–oxygen bonds (Maity et al., 2009; Pan et al., 2014; Lam et al., 2020).

3.5 Catalytic tests

The conversion of palm oil consists of several steps. First, the double bonds in the triglycerides of palm oil are hydrogenated by a

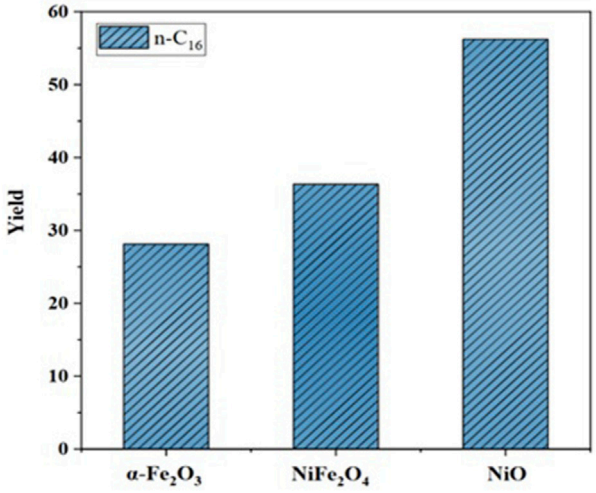

FIGURE 7
Yields to "green diesel" of the n-alkane (n-C_{16}) generated by all the nanocatalysts in the deoxygenation of palm oil. (350 C, 3.5 MPa initial H_2 pressure, and 3 h reaction).

catalyst to form saturated triglycerides. Then, the C–O bond in saturated triglycerides is disengaged by hydrogenolysis to generate fatty acids and propane (Ruangudomsakul et al., 2022). The catalytic deoxygenation of palmitic acid can be performed in three ways (Figure 6). Hydrodeoxygenation can mainly occur, eliminating oxygen in the form of H_2O through the cleavage of the C–O bond in the presence of hydrogen. Similarly, oxygen can be eliminated by the formation of CO and/or CO_2 through the disengagement of the C–C bond (Choi et al., 2018). In all three cases, reactions are promoted in the presence of a catalyst; to improve the performance of the reaction, a solvent is used with a lower boiling point than oil to promote better activity (Di Vito Nolfi et al., 2021). In addition, the presence of a solvent also affects the performance of the reaction, allowing a high diffusivity that reduces resistance to the mass transfer of the reagents by facilitating the contact of the H_2 and reagents with the catalyst (Lucantonio et al., 2023). The solvent content considerably increased the pressure due to isothermal expansion during the reaction. The used condition reaction (350 °C for 3 h and 3.5 MPa of H2 pressure) promoted the selectivity to n-C16 detected during the reaction.

The catalytic evaluation showed that the most active material in the formation of hydrocarbons in the n-C_{16} range was NiO (the highest yield nearly 56%) due to high activation of hydrogenation and the fragmentation of the side chains of triglycerides. Small nickel particles with particularly active sites such as steps, corners, and defects tend to deoxygenate C–O bonds (Chen et al., 2016; Mortensen et al., 2016; Shafaghat et al., 2016; Wang et al., 2018; KretzschmarOliverSeifert, 2024). The $NiFe_2O_4$ nanocatalysts obtain 35% yield, thus promoting action attributed to the synergy of the nickel and iron sites but lower than NiO nanoparticles. Finally, the α-Fe_2O_3 nanocatalysts showed a decrease compared to the NiO and $NiFe_2O_4$ catalysts because iron without a hydrogen activation site does not completely promote hydrogenation. Therefore, the efficiency of the deoxygenation of fatty acids in producing n-C_{16} hydrocarbons has the following order: α-Fe_2O_3 < $NiFe_2O_4$ < NiO (Figure 7).

4 Conclusion

These results demonstrate a viable, fast, economical, and promising route for the synthesis of α-Fe_2O_3, $NiFe_2O_4$, and NiO catalysts at the nanometer scale. Iron can considerably decrease the particle size of Ni, forming a ferrite-type structure; However, this hot injection method promotes the formation of nickel nanoparticles (less than 50 nm) and aggregated particle sizes from 100 to 160 nm. Catalytic evaluation confirmed that a catalyst promoted by Ni facilitates a greater degree of deoxygenation. The reaction conditions are considered appropriate (350 C, 3 h, and 3.5 MPa initial H2 pressure) for generating n-alkanes (n-C16) in the diesel range. In all experimental processes, n-C16 was obtained as the main product, with the presence of other products with a greater added value than the oil source.

Data availability statement

The original contributions presented in the study are included in the article/Supplementary material; further inquiries can be directed to the corresponding author.

Author contributions

JM-B: conceptualization, investigation, methodology, project administration, validation, formal analysis, funding acquisition, resources, and writing–review and editing. CG-C: formal analysis, investigation, methodology, and writing–original draft. ML-M: investigation, supervision, and writing–review and editing. ND-Z: investigation, validation, and writing–review and editing. LV-I: investigation, writing–review and editing, and supervision. MM-M: data curation, supervision, and writing–review and editing.

Funding

The author(s) declare financial support was received for the research, authorship, and/or publication of this article. The authors acknowledge project 19000.23-P from Tecnológico Nacional de México for financial support.

Conflict of interest

The authors declare that the research was conducted in the absence of any commercial or financial relationships that could be construed as a potential conflict of interest.

Publisher's note

References

Babu, L. K., and Reddy, Y. V. R. (2020). A novel thermal decomposition approach for the synthesis and properties of superparamagnetic nanocrystalline $NiFe_2O_4$ and its antibacterial, electrocatalytic properties. *J. Supercond. Nov. Magn.* 33 (4), 1013–1021. doi:10.1007/s10948-019-05262-x

Belaïd, S., Laurent, S., Vermeech, M., Vander Elst, L., Perez-Morga, D., and Muller, R. N. (2013). A new approach to follow the formation of iron oxide nanoparticles synthesized by thermal decomposition. *Nanotechnology* 24 (5), 055705. doi:10.1088/0957-4484/24/5/055705

Chen, L., Li, H., Fu, J., Miao, C., Lv, P., and Yuan, Z. (2016). Catalytic hydroprocessing of fatty acid methyl esters to renewable alkane fuels over Ni/HZSM-5 catalyst. *Today* 259 (1), 266–276. Part 2. doi:10.1016/j.cattod.2015.08.023

Choi, I.-H., Lee, J.-S., Kim, C.-U., Kim, T.-W., Lee, K.-Y., and Hwang, K.-R. (2018). Production of bio-jet fuel range alkanes from catalytic deoxygenation of Jatropha fatty acids on a $WOx/Pt/TiO_2$ catalyst. *Fuel (Lond)* 215, 675–685. doi:10.1016/j.fuel.2017.11.094

Cullity, B. D., and Stock, S. R. (2013). *Elements of X-ray diffraction: pearson new international edition*. 3. London, England: Pearson Education.

Demirbas, A. (2004). Bioenergy, global warming, and environmental impacts. *Energy sources.* 26 (3), 225–236. doi:10.1080/00908310490256581

Demirbas, A., and Dincer, K. (2008). Sustainable green diesel: a futuristic view. *Energy Sources Recovery Util. Environ. Eff.* 30 (13), 1233–1241. doi:10.1080/15567030601082829

Dippong, T., Levei, E. A., and Cadar, O. (2021). Recent advances in synthesis and applications of MFe_2O_4 (M = co, Cu, Mn, Ni, Zn) nanoparticles. *Nanomater. (Basel)* 11 (6), 1560. doi:10.3390/nano11061560

Di Vito Nolfi, G., Gallucci, K., and Rossi, L. (2021). Green diesel production by catalytic hydrodeoxygenation of vegetables oils. *Int. J. Environ. Res. Public Health* 18 (24), 13041. doi:10.3390/ijerph182413041

Gong, S., Shinozaki, A., Shi, M., and Qian, E. W. (2012). Hydrotreating of Jatropha oil over alumina based catalysts. *Energy fuels.* 26 (4), 2394–2399. doi:10.1021/ef300047a

Gutierrez, A., Perpiñán, M. F., Sánchez, A. E., and Torralba, M. C. (2013). Solvotermal synthesis of NiO, Ni and NiS nanoparticles. *J. Nanosci. Nanotechnol.* 13 (1), 461–466. doi:10.1166/jnn.2013.6717

Guzman, A., Torres, J. E., Prada, L. P., and Nuñez, M. L. (2010). Hydroprocessing of crude palm oil at pilot plant scale. *Catal. Today* 156 (1–2), 38–43. doi:10.1016/j.cattod.2009.11.015

Kim, S. K., Brand, S., Lee, H.-S., Kim, Y., and Kim, J. (2013). Production of renewable diesel by hydrotreatment of soybean oil: effect of reaction parameters. *Chem. Eng. J.* 228, 114–123. doi:10.1016/j.cej.2013.04.095

Kovács, S., Kasza, T., Thernesz, A., Horváth, I. W., and Hancsók, J. (2011). Fuel production by hydrotreating of triglycerides on $NiMo/Al_2O_3$/Fcatalyst. *Chem. Eng. J.* 176–177, 237–243. doi:10.1016/j.cej.2011.05.110

KretzschmarOliverSeifert, N. B. M. (2024). Controlling the reaction network of Ni/silica derived conversion of bio-oil surrogate guaiacol. *Carbon Resour. Convers.* 7, 100187. doi:10.1016/j.crcon.2023.05.006

Kubička, D., Horáček, J., Setnička, M., Bulánek, R., Zukal, A., and Kubičková, I. (2014). Effect of support-active phase interactions on the catalyst activity and selectivity in deoxygenation of triglycerides. *Appl. Catal. B* 145, 101–107. doi:10.1016/j.apcatb.2013.01.012

Kurtan, U., Güngüneş, H., Sözeri, H., and Baykal, A. (2016). Synthesis and characterization of monodisperse $NiFe_2O_4$ nanoparticles. *Ceram. Int.* 42 (7), 7987–7992. doi:10.1016/j.ceramint.2016.01.200

Lam, M. M., Melo-Banda, J. A., Macias, F. D., Portales, B., Dominguez, J. M., Silva, R., et al. (2020). Transition metal nanocatalysts by modified inverse microemulsion for the heavy crude oil upgrading at reservoir. *Catal. Today* 349, 81–87. doi:10.1016/j.cattod.2018.05.052

Lucantonio, S., Di Giuliano, A., Rossi, L., and Gallucci, K. (2023). Green diesel production via deoxygenation process: a review. *Energies* 16 (2), 844. doi:10.3390/en16020844

Maity, D., Choo, S.-G., Yi, J., Ding, J., and Xue, J. M. (2009). Synthesis of magnetite nanoparticles via a solvent-free thermal decomposition route. *J. Magn. Magn. Mater* 321 (9), 1256–1259. doi:10.1016/j.jmmm.2008.11.013

Morgan, T., Santillan-Jimenez, E., Harman-Ware, A. E., Ji, Y., Grubb, D., and Crocker, M. (2012). Catalytic deoxygenation of triglycerides to hydrocarbons over supported nickel catalysts. *Chem. Eng. J.* 189–190, 346–355. doi:10.1016/j.cej.2012.02.027

Mortensen, P. M., Grunwaldt, J.-D., Jensen, P. A., and Jensen, A. D. (2016). Influence on nickel particle size on the hydrodeoxygenation of phenol over Ni/SiO2. *Catal. Today* 259 (1), 277–284. Part 2. doi:10.1016/j.cattod.2015.08.022

Mourdikoudis, S., and Liz-Marzán, L. M. (2013). Oleylamine in nanoparticle synthesis. *Chem. Mater* 25 (9), 1465–1476. doi:10.1021/cm4000476

Pan, Y., Jia, R., Zhao, J., Liang, J., Liu, Y., and Liu, C. (2014). Size-controlled synthesis of monodisperse nickel nanoparticles and investigation of their magnetic and catalytic properties. *Appl. Surf. Sci.* 316, 276–285. doi:10.1016/j.apsusc.2014.07.203

Ruangudomsakul, M., Osakoo, N., Wittayakun, J., Keawkumay, C., Butburee, T., Youngjan, S., et al. (2022). Hydrodeoxygenation of palm oil to green diesel products on mixed-phase nickel phosphides. *Mol. Catal.* 523 (111422), 111422. doi:10.1016/j.mcat.2021.111422

Shafaghat, H., Sirous Rezaei, P., Ashri, W. M., and Wan DaudRezaei, P. S. (2016). Catalytichydrodeoxygenation of simulated phenolic bio-oil to cycloalkanes and aromatic hydrocarbons over bifunctional metal/acid catalysts of Ni/HBeta, Fe/HBeta and NiFe/HBeta. *J. Industrial Eng. Chem.* 35, 268–276. doi:10.1016/j.jiec.2016.01.001

Srifa, A., Faungnawakij, K., Itthibenchapong, V., and Assabumrungrat, S. (2015a). Roles of monometallic catalysts in hydrodeoxygenation of palm oil to green diesel. *Chem. Eng. J.* 278, 249–258. doi:10.1016/j.cej.2014.09.106

Srifa, A., Faungnawakij, K., Itthibenchapong, V., Viriya-Empikul, N., Charinpanitkul, T., and Assabumrungrat, S. (2014). Production of bio-hydrogenated diesel by catalytic hydrotreating of palm oil over NiMoS2/γ-Al2O3 catalyst. *Bioresour. Technol.* 158, 81–90. doi:10.1016/j.biortech.2014.01.100

Srifa, A., Viriya-empikul, N., Assabumrungrat, S., and Faungnawakij, K. (2015b). Catalytic behaviors of $Ni/\gamma\text{-}Al_2O_3$and $Co/\gamma\text{-}Al_2O_3$ during the hydrodeoxygenation of palm oil. *Catal. Sci. Technol.* 5 (7), 3693–3705. doi:10.1039/c5cy00425j

Vonortas, A., and Papayannakos, N. (2014). Comparative analysis of biodiesel versus green diesel: comparative analysis of biodiesel versus green diesel. *Wiley Interdiscip. Rev. Energy Environ.* 3 (1), 3–23. doi:10.1002/wene.78

Wang, X., Zhu, S., Wang, S., Wang, J., Fan, W., and Lv, Y. (2018). Ni nanoparticles entrapped in nickel phyllosilicate for selective hydrogenation of guaiacol to 2-methoxycyclohexanol. *Appl. Catal. A General* 568 (25), 231–241. doi:10.1016/j.apcata.2018.10.009

Zhai, X., Zhang, X., Chen, S., Yang, W., and Gong, Z. (2012). Oleylamine as solvent and stabilizer to synthesize shape-controlled ZnS nanocrystals with good optical properties. *Colloids Surf. A Physicochem Eng. Asp.* 409, 126–129. doi:10.1016/j.colsurfa.2012.05.047